ISSN 1022 - 2502, E-ISSN 2408- 8528
Dhaka Univ. J. Sci. 69(2): 88-95, 2021 (July) DOI: https://doi.org/10.3329/dujs.v69i2.56488

Performance Enhancement of an a-Si:H/μc-Si:H Heterojunction p-i-n Solar Cell by Tuning the Device Parameters

Md. Nazmul Islam Sarkar and Himangshu Ranjan Ghosh*

Institute of Energy, University of Dhaka, Dhaka 1000, Bangladesh

(Received : 26 June 2021; Accepted: 14 October 2021)

Abstract

In this work, the solar cell design parameters like- layer thickness, bandgap, donor and acceptor concentrations are varied to find optimum structure of a hydrogenated amorphous silicon (a-Si:H) and hydrogenated microcrystalline silicon (µc-Si:H) heterojunction p-i-n solar cell. A thin a-Si:H p-layer of 1 to 5 nm followed by a thick a-Si:H i-layer of thickness 1400 to 1600 nm and then thin n-layer of thickness 1 to 5 nm with acceptor concentration of 102 cm^{-3} and donor concentration of 1020 cm−3 and the bandgaps of p-, i-, and n- layers with higher bandgaps closer to 2.2 eV for a-Si:H p-layer, 1.85 eV for a-Si:H i-layer, and 1.2 eV for µc-Si:H n-layer have showed better performances. The optimum cell has a J_{SC} of 18.93 mA/cm^2, V_{OC} of 1095 mV, Fill factor of 0.7124, and efficiency of 14.77%. The overall external quantum efficiency of the numerically designed cell also remained very high from 85-95 % for wavelengths of 300-650 nm range. This indicates that the device will perform its best under both high and low frequency i.e. ultra-violet, near visible and visible light wavelengths.

Keywords: Heterojunction solar cell, p-i-n solar cell, solar cell simulation and optimization

I. Introduction

Amorphous silicon (a-Si) or its hydrogenated form (a-Si:H) has long range of disorder in the silicon network and momentum conservation law for electron excitation by photon absorption is relaxed and hence it does not need phonon for electronic transitions or behaves like a direct bandgap material (1.5- 2.2 eV, depending on deposition conditions and percentage of hydrogen).[1] Due to the direct bandgap properties, amorphous silicon has higher light absorption coefficient than that of crystalline silicon nd thin (around 1-micrometre) film solar cells can be made by it. [2-5] In the arena of a-Si:H based solar cell, microcrystalline silicon (μc-Si:H having indirect bandgap ~1.1eV) is also used which is characterized by its nanoscale crystal structures, in the range of 20–700 nm with different orientations and has favorable optical and electrical properties, like low optical absorption in the ultra- violet–visible– near-infrared range and high conductivity and doping efficiency.[1] These a-Si:H and/or μc-Si:H based thin film solar cells are getting popularity than that of self-supporting bulk wafer based silicon solar cells for their low material consumption, therefore reduce cost, low temperature processing, deposition facilities on glass or any other flexible plastic/metal foils and potential of multi-junction or tandem solar cells.[6-10]

Yunaz et al. found a potential efficiency over 20% for the Si-based multijunction thin film solar cell.[12] Another groups have integrated a-Si:H and hydrogenated microcrystalline silicon (μc-Si:H) absorbers into tandem structure cells with a stabilized efficiency over 10%.[13,14] Moreover, Yan et al. have reported an a-Si:H/a-SiGe:H/μc-Si:H triple-junction cell reached a recorded efficiency of 16.3%.[15] Tandem and multijunction solar cells are a great solution to reach more than 30% efficiency. With their high power conversion efficiencies over 25%, silicon heterojunction solar cells (SHJ) are very promising candidates as bottom-cell for monolithic tandem solar cells.[16] Ding et al.[17] have optimized amorphous silicon oxide buffer layers for silicon heterojunction solar cells. Ge et al.[18] have optimized intrinsic a-Si: H passivation layers in crystalline-amorphous silicon heterojunction solar cells. However, there is lack of studies of optimization of device parameters for efficiency improvement of a-Si:H/μc-Si:H hetero-junction solar cells.

In this work, the device parameters like- layer thickness, bandgap, donor and acceptor concentrations are varied to find structure, optimum optical and electrical performance of a-Si:H/μc-Si:H heterojunction solar cell using numerical simulation software AFORS-HET.

II. Methodology

Numerical modeling

A set of equations govern the operation of semiconductor devices provides the ideal characteristics for solar cells, i.e., the current density equation, Poisson's equation and the continuity equation.[19,20] The total current density of electrons and holes in doped semiconductors includes both the drift and diffusion currents. One (x) dimensional equations are given below.

$$J_n = qn(x)\mu_n E(x) + qD_n \frac{dn}{dx} \quad (1a)$$

$$J_p = qp(x)\mu_p E(x) - qD_p \frac{dp}{dx} \quad (1b)$$

Where, J_n and J_p are the current densities due to mobile electrons and holes respectively; n and p are the concentration of mobile electrons and holes respectively; q is absolute charge of each electron and hole; μ_n and μ_p are mobility of electrons and holes respectively; E is the electric field intensity voltage/length; D_n and D_p are diffusion constants for electrons holes respectively.

Maxwell's equations of electromagnetic field theory shows that free electric charges gives rise to an electric field in the semiconductor through Poisson's equation (equation2).

*Author for correspondence. e-mail: *hrghosh@du.ac.bd*

$$\frac{d^2\varphi}{dx^2} = -\frac{q}{\varepsilon}(p - n + N_d^+ - N_a^-) \quad (2)$$

Where, φ is the electric potential; N_d^+ and Na^- are the concentrations of ionized donors and acceptors; ε is the material's permittivity (an intrinsic property measuring the resistance to the forming of an electric field).

This next set of equations is beneficial for keeping track of particles moving in and out of a given volume of the semiconductor to ensure that the particles passing through a given volume, are being generated and recombined appropriately in order to account for changes in flow rate within the volume. These equations are basically particle conservation equations.

$$\frac{dn}{dt} = \frac{1}{q}\frac{dJ_n}{dx} + G_n - R_n \quad (3a)$$

$$\frac{dp}{dt} = -\frac{1}{q}\frac{dJ_p}{dx} + G_p - R_p \quad (3b)$$

Where, t is the time; G and R represent carrier generation and recombination rates.

Simulation

Based on the basic and relevant semiconductor equations for defects and others in numerical modeling section, appropriate boundary and steady-state conditions with small sinusoidal perturbations are applied in **A**utomat **for** **s**imulation of **het**erostructures (Version 2.5, AFORS-HET[21], Helmholtz-Zentrum Berlin für Materialien und Energie) to simulate one dimensional semiconductor structures by numerical methods.[8] To do this, the coupled partial differential equations set is transformed into non-linear algebraic equations set by finite difference methods.

P type or or n type amorphous silicon has high density of dangling bonds. Generated carriers are lost by recombination and hence amorphous silicon solar cells prefer p-i-n (or n-i-p) structures to prepare the electric field in the intrinsic region (i region) and drift carriers to the external contacts.[22] In the proposed solar cell, glass is used as the substrate followed by a thin transparent conducting oxide (TCO), a thin a-Si:H p-, i-, and followed by μc-Si:H n-layer with metal contacts at the back side. Indian tin oxide (ITO) or ZnO can be used as TCO and Al as the back contact as shown in Figure 1.

In both a-Si:H and μc-Si:H material there are disordered regions and voids.[23] To model these amorphous and microcrystalline structures the density of states has been assumed to be both acceptor like states (in the upper half of the gap) and donor like states (in the lower half of the gap). Both of these acceptor and donor like states consist of exponential band tail and Gaussian mid-gap states, shown in Figure 2.

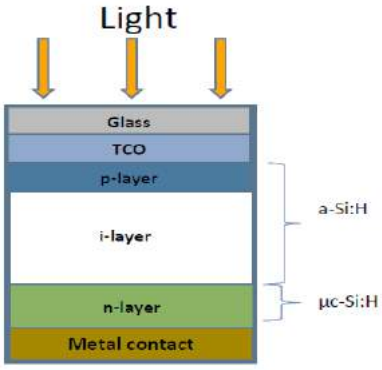

Fig. 1. Schematic diagram of a-Si:H/μc-Si:H heterojunction solar cell

Input parameters of the baseline a-Si:H and μc-Si:H p-i-n heterostructure used in the simulations are given in Table 1. For simulation all the default values of AFORS-HET were adopted, unless otherwise stated in this table.[24]

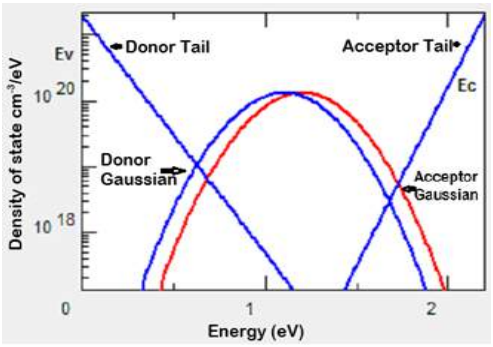

(a) a-Si:H p-layer

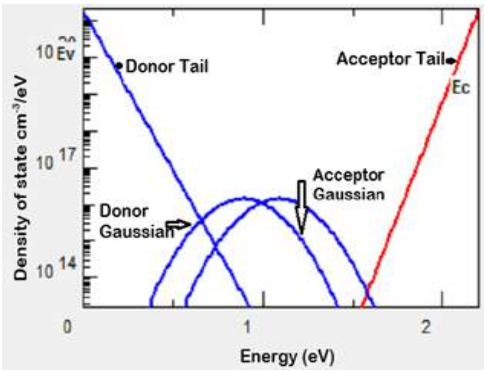

(b) a-Si:H i-layer

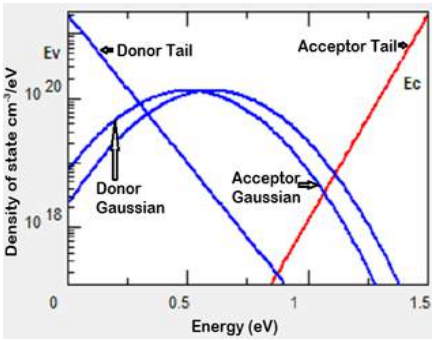

(c) µc-Si:H n-layer

Fig. 2. Defect state distributions of a-Si:H p-, i-, and _c-Si:H n-layers of the cell

Table 1. Input parameters of the baseline a-Si:H and *μ*c-Si:H p-i-n heterostructure cell

Parameters	a-Si:H p-layer	a-Si:H i-layer	uc-Si:H n-layer
Layer thickness, L(nm)	variable	variable	variable
Dielectric constant	11.9	11.9	11.9
Bandgap, Eg (eV)	variable	variable	variable
Electron mobility	20	20	50
Hole mobility	5	5	5
Acceptor concentration, Na(cm^{-3})	variable	0	0
Donator concentration, Nd (cm^{-3})	0	1000	variable
Effective DOS CB, Nc (cm^{-3})	1.00E+20	1.00E+20	1.00E+19
Effective DOS VB, Nv (cm^{-3})	1.00E+20	1.00E+20	1.00E+19
Electron affinity (eV)	3.9	3.9	3.9
Valence Band tail states parameters			
VB trap density (cm^{-3})	2.40E+20	9.40E+19	1.88E+20
VB tail characteristic energy (meV)	120	50	94
Electron capture cross section (cm^2)	7.00E-16	7.00E-16	7.00E-16
Hole capture cross section (cm^2)	7.00E-16	7.00E-16	7.00E-16
Conduction Band tail states parameters			
CB trap density (cm^{-3})	1.60E+20	6.40E+19	1.36E+20
CB tail characteristic energy (meV)	80.00	35.00	68.00
Electron capture cross section (cm^2)	7.00E-16	7.00E-16	7.00E-16
Hole capture cross section (cm^2)	7.00E-16	7.00E-16	7.00E-16
Gaussian defect states parameters (Acceptor)			
Defect density (cm^{-3})	6.90E+19	5.00E+15	6.90E+19
Standard deviation (Gaussian) (eV)	0.21	0.144	0.21
Electron capture cross section (cm^2)	3.00E-15	3.00E-15	3.00E-15
Hole capture cross section (cm^2)	3.00E-14	3.00E-14	3.00E-14
Gaussian defect states parameters (Donor)			
Defect density (cm^{-3})	6.90E+19	5.00E+15	6.90E+19
Standard deviation (Gaussian) (eV)	0.21	0.144	0.21
Electron capture cross section (cm^2)	3.00E-14	3.00E-15	3.00E-14
Hole capture cross section (cm^2)	3.00E-15	3.00E-14	3.00E-14

Microcrystalline silicon shows somewhat lower effective conduction band density (N_c) and valence band density (N_v) for the presence of crystalline grains in the material. That is why values of N_c and N_v are kept one order lower than that of amorphous silicon. For the same reason electron mobility and hole mobility are also kept little higher.

The efficiency, short circuit current density, open circuit voltage, and fill factor of the hetero-structure p-i-n device depend on design parameters like window layer thickness, donor and acceptor concentrations, electron and hole mobility, band-gap, and band-tail states. However, both amorphous and microcrystalline silicon have low mobility and large number of localized gap states which reduces the efficiency significantly. In this work, the input parameters like layer thickness, bandgap, donor and acceptor concentrations are varied to find best performed cell structure. Later on, the performance of the optimized a-Si:H/μc-Si:H heterojunction solar cell is validated at a device temperature T = 300K. AM 1.5 spectrum with 100 mW/cm^2 illumination. Light is imposed from the top side of the cell as shown in Figure 1.

III. Results and Discussions

Optimization of layer thickness

Layer thickness plays an important role in the optimization of a thin film p-i-n device. As a-Si:H p-layer is actually the window layer, its thickness is varied from 1 nm - 100 nm. It is essential to have a thick intrinsic layer, which acts as a buffer layer for better absorption of photons. Therefore, a-Si:H i-layer is varied from several nanometers to 5 micrometers. The µc-Si:H n-layer is kept within the 1 to 200 nm range and varied to find the optimum thickness for better electron transport as in Figure 3 .

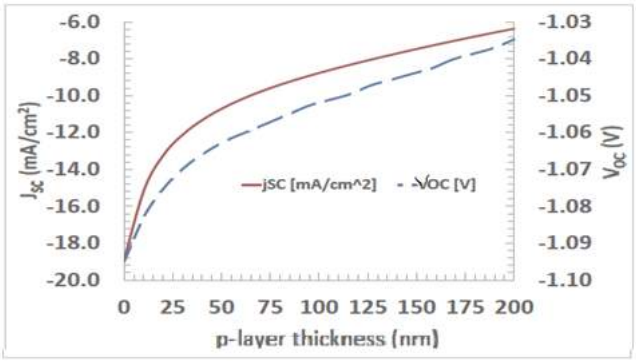

(a) J_{SC} and V_{OC} with a-Si:H p-layer thickness

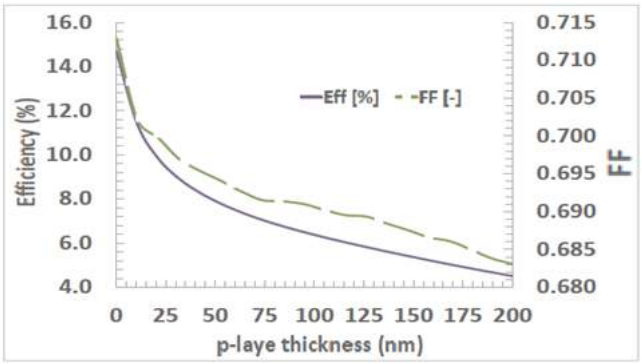

(b) Efficiency and FF with a-Si:H p-layer thickness

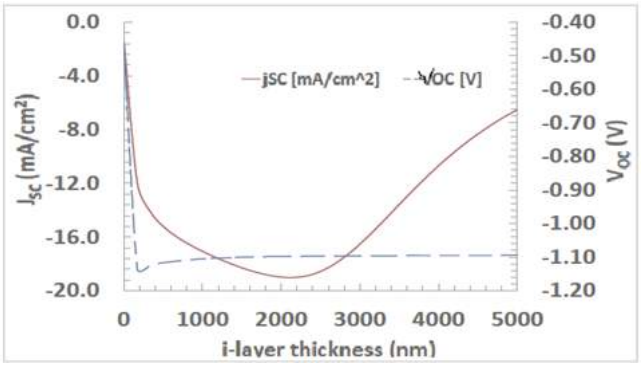

(c) J_{SC} and V_{OC} with a-Si:H i-layer thickness

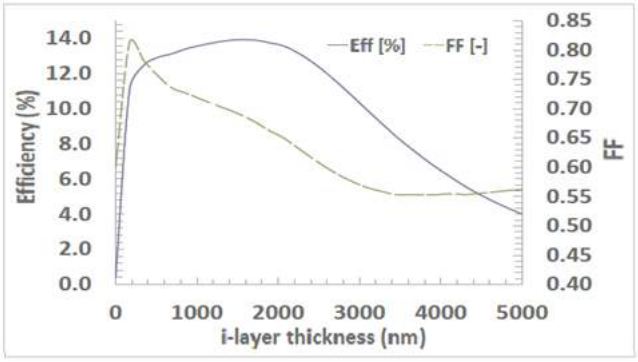

(d) Efficiency and FF with a-Si:H i-layer thickness

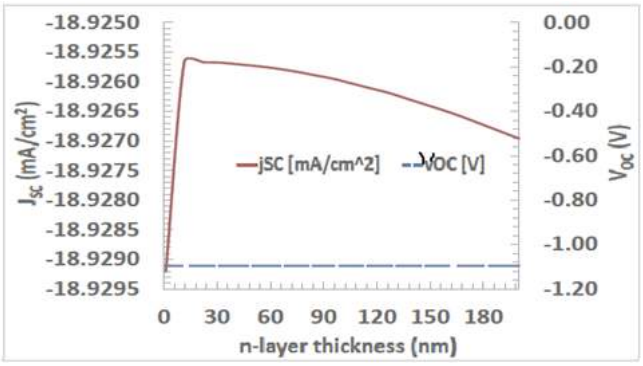

(e) J_{SC} and V_{OC} with µc-Si:H n-layer thickness

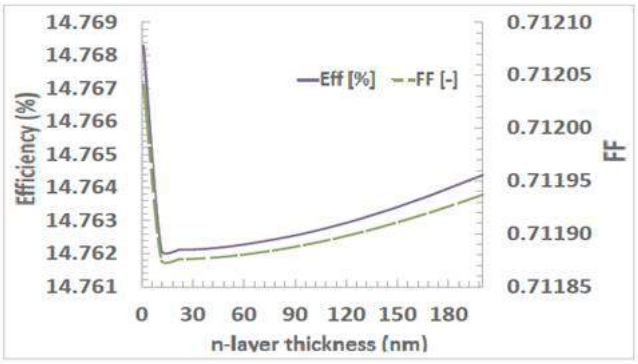

(f) Efficiency and FF with µc-Si:H n-layer thickness

Fig. 3. Effect of thickness variation on J_{SC} and V_{OC} are shown in (a), (c), and (e) for a-Si:H p-, i-, and µc-Si:H n-layer respectively. Variation in efficiency and FF are shown in (b), (d), and (f) for a-Si:H p-, i-, and μc-Si:H n-layer respectively

Figure 3 illustrates the effect of thickness variation on J_{SC}, V_{OC}, FF, and Efficiency. From Figure 3(a) and 3(b) it is evident that a thin a-Si:H p-layer of 1 to 5 nm would result in a better J_{SC}, and V_{OC}, and thus a higher efficiency. With increase in thickness of p-layer the amount of light reaching the absorber layer reduces and results in lower J_{SC} values. It also becomes difficult for the built in field to separate the electron-hole pair if the thickness of p-layer is high.

On the other hand, from Figure 3(c) and 3(d) it can be seen that an a-Si:H absorber layer of 1400 to 1800 nm should be used to get better performance from the device. With increase of i-layer thickness J_{SC} increases gradually up to 2 μm but starts decreasing after that. However, V_{OC} increases abruptly just after 10 nm and reaches to its maximum value after 100 nm and remains almost constant for further increase in thickness.

For μc-Si:H n-layer the maximum efficiency can be achieved within 1 to 10 nm range where efficiency and FF are maximum as shown in Figure 3(e) and 3(f). Although J_{SC} decreases with increase of thickness, V_{OC} remains constant throughout the variation. This is because of the lower electron and hole mobility of the a-Si:H where thicker n-layers reduces the electron transport facility.

Optimization of doping concentrations

Variation of efficiency along with J_{SC}, V_{OC} and FF are depicted in Figure 4 for the variation in acceptor and donor concentration. From Figure 4(a) it can be seen that V_{OC} and J_{SC} both increases with increase in a-Si:H p-layer acceptor concentration, N_a. However, beyond the acceptor concentration of $10^{19}\ cm^{-3}$, the V_{OC} and J_{SC} both reached the maximum value and do not increase further. This is because of the fully crowded states in the cell, which saturates the performance. For this reason it is also seen from Figure 4(b) that efficiency and FF also reached to saturation after the $10^{19}\ cm^{-3}$ limit.

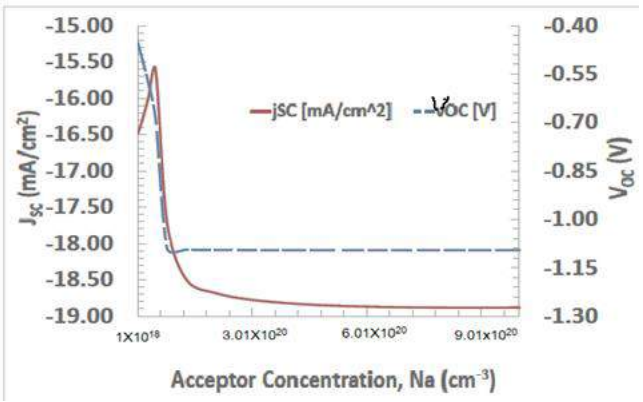

(a) Effect of a-Si:H p-layer N_a variation on J_{SC} and V_{OC}

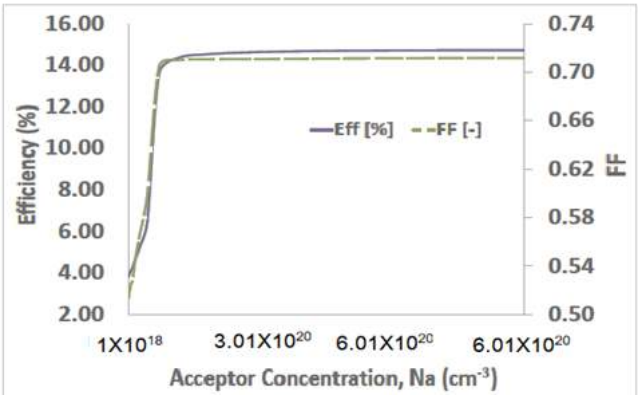

(b) Effect of a-Si:H p-leayer N_a variation on Efficiency and FF

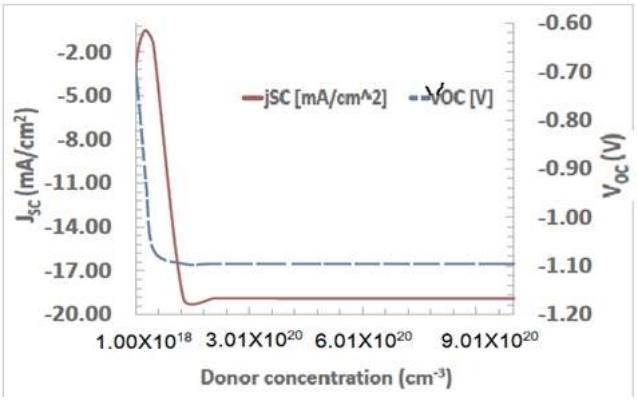

(c) Effect of μc-Si:H n-layer N_d variation on J_{SC} and V_{OC}

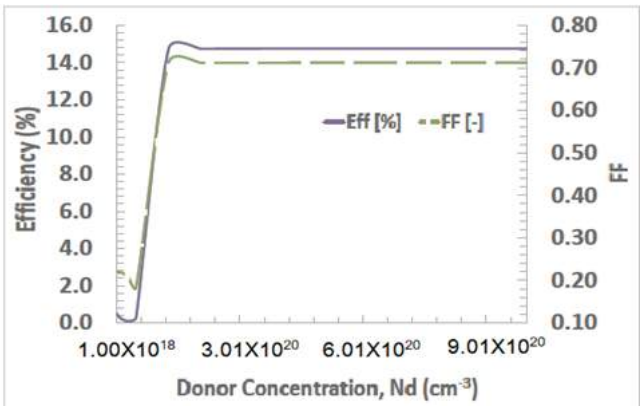

(d) Effect of μc-Si:H n-layer N_d variation on Efficiency and FF

Fig. 4. Impact of Acceptor concentration (N_a) and Donor concentration (N_d) variation on J_{SC}, V_{OC}, Efficiency and FF

From Figure 4(a) it can be seen that V_{OC} and J_{SC} both increases with increase in a-Si:H p-layer acceptor concentration, N_a. However, beyond the acceptor concentration of 10^{19} cm^{-3}, the V_{OC} and J_{SC} both reached the maximum value and do not increase further. This is because of the fully crowded states in the cell, which saturates the performance. For this reason it is also seen from Figure 4(b) that efficiency and FF also reached to saturation after the 10^{19} cm^{-3} limit.

In the case of μc-Si:H n-layer donor concentration, N_d from Figure 4(c) and 4(d) it can be seen that V_{OC} and J_{SC} both increase till 10^{19} cm^{-3} but beyond that range V_{OC} and J_{SC} both do not increase that much and the device saturates. Increasing donor concentration further does not increase the efficiency and FF.

Optimization of Bandgaps

Bandgaps of the a-Si:H p-, i-, and μc-Si:H n-layers are varied to find the optimum bandgaps for the heterojunction p-i-n device. For a-Si:H the bandgap can be varied from 1.5 to 2.2 eV and for μc-Si:H from 1.2 eV to 1.5 eV.[2,3,27] The bandgaps of p-, i-, and n-layers were varied in the specified range for optimization. Effect of bandgap variation on J_{SC} and V_{OC}, efficiency and FF are shown in Figure 5.

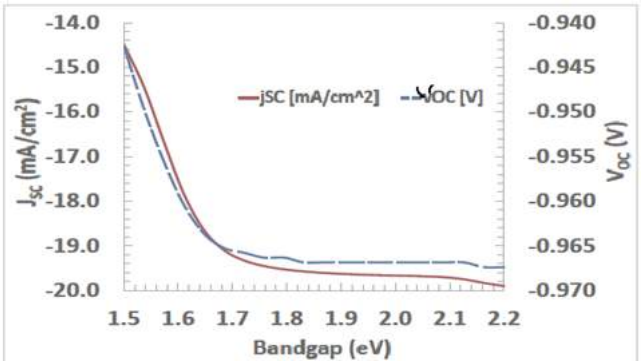

(a) J_{SC} and V_{OC} with a-Si:H p-layer bandgap

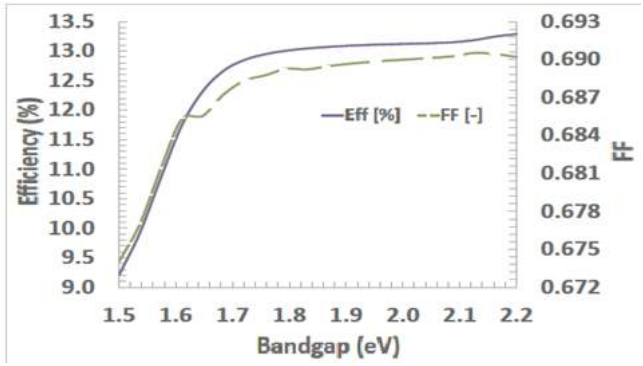

(b) Efficiency and FF with a-Si:H p-layer bandgap

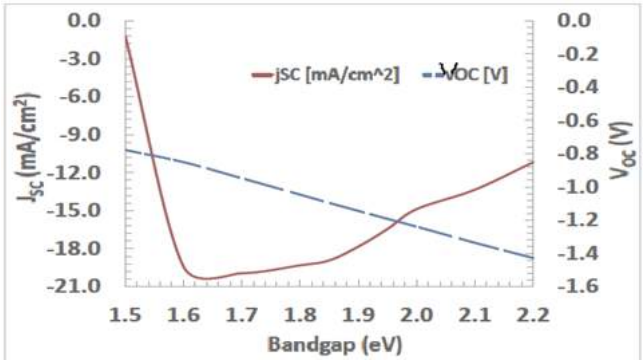

(c) J_{SC} and V_{OC} with a-Si:H i-layer bandgap

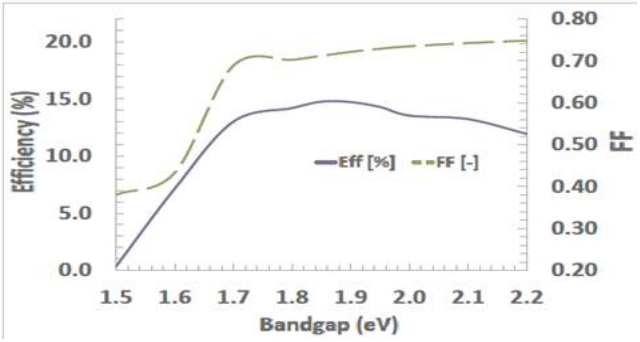

(d) Efficiency and FF with a-Si:H i-layer bandgap

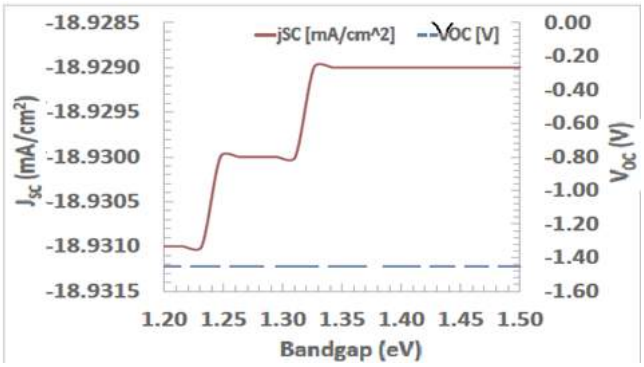

(e) J_{SC} and V_{OC} with μc-Si:H n-layer bandgap

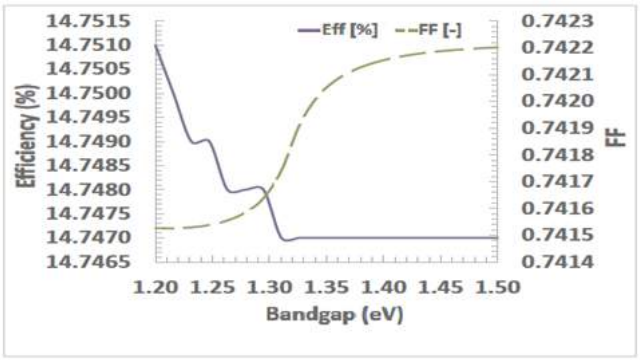

(f) Efficiency and FF with μc -Si:H n-layer bandgap

Fig. 5. Effect of bandgap variation on J_{SC} and V_{OC} are shown in (a), (c), and (e) for a-Si:H p-, i-, and c-Si:H n-layer respectively. Variation in efficiency and FF are shown in (b), (d), for a-Si:H p-and i-layers and in (f) for μc -Si:H n-layer respectively

It can be seen from Figure 5(a) and 5(b) that J_{SC} and V_{OC} both reaches to its maximum value with a higher bandgap of the a-Si:H window layer close to 2.1 eV. This is because with increase in p-layer bandgap more photons can reach the absorber layer to produce more current. It can also be seen that the V_{OC} also follows the similar trend. The reason why V_{OC} also increases can be the lower rate of recombination with higher badgap of window layer. Therefore, both efficiency and FF also reached their maximum value above 2.0 eV bandgap of p-layer.

For a-Si:H i-layer bandgap variation from 1.5 eV to 2.2 eV it can be seen from Figure 5(c) and 5(d) that J_{SC} increases abruptly with increase in i-layer bandgap from 1.5 eV to 1.6 eV. However, it starts to decrease after 1.8 eV. On the other hand, V_{OC} has an approximately linear increasing trend with increase in bandgap. This might be because of the lowering of band offset with increase in bandgap of i-layer. As bandgap of p layer is kept at 2.1 eV, the low bandgap of i-layer would create a band offset which will eventually increase the recombination. Therefore, maximum efficiency is achieved within the 1.8 to 1.9 eV range.

From Figure 5(e) and 5(f) it can be seen that J_{SC} decreases with increase of μc-Si:H n-layer bandgap and after 1.35 eV the device reaches saturation. However, V_{OC} remains constant throughout the variation of n-layer. Therefore maximum efficiency is achieved close to the μc-Si:H n-layer bandgap of 1.2eV.

Optimized cell performance

By taking all the optimal values of the layer thicknesses, bandgap, and doping concentrations of both a-Si:H p- and i-layer and μc-Si:H n-layer and running the simulation using AFORS-HET the characteristics of the best performed heterojunction cell was found. Table 2 shows the optimum parameters found in the simulation and used to design the best-performed p-i-n cell. Here it is noticed that the top a-Si:H p layer has acted as an window layer by picking its highest possible bandgap, 2.2 eV.

Illumination of 1000 W/m^2 at AM 1.5 was used to find the J-V and P-V curves shown in Figure 6. The calculated light J-V characteristics of the cell yield the following results.

- Short circuit current density of J_{SC} = -18.93 mA/cm^2,
- Open circuit voltage V_{OC} = -1095 mV ,
- Fill-factor, FF = 0.7124,
- Efficiency = 14.77 %.

Figure 7 shows the band diagram of the optimum heterostructure p-i-n cell under equilibrium condition. The fermi level was found to be at -6.15 eV.

Table 2. Optimum parameters found in simulation and used to design the best-performed cell

Layers	Thickness, L(nm)	N*a* (cm^{-3})	N*d* (cm^{-3})	Eg (eV)
a-Si:H p-layer	1	1×10^{21}	0	2.2
a-Si:H i-layer	1600	0	1000	1.85
μc-Si:H n-layer	1	0	1×10^{20}	1.2

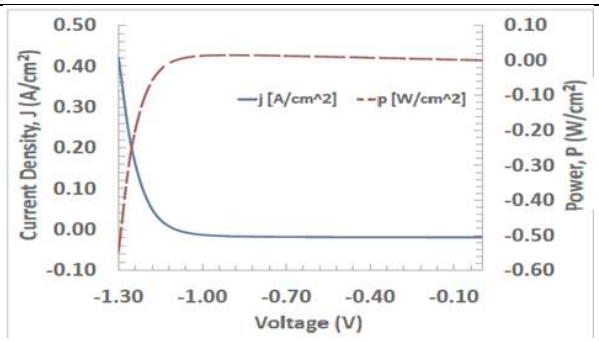

Fig. 6. J-V and P-V curve of the best performed p-i-n cell under AM 1.5 spectrum and 1000 *W/m*^{2} illumination

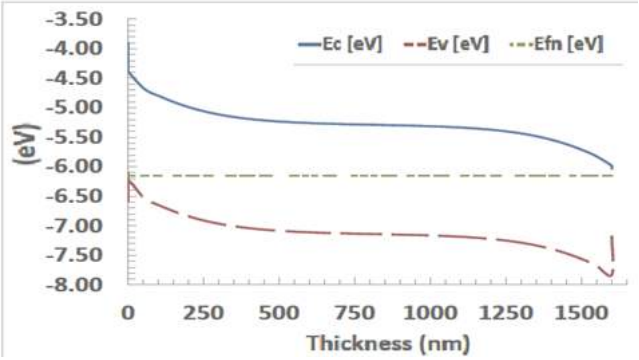

Fig. 7. Band diagram of the optimum cell under equilibrium condition

The generation and recombination rate of the designed cell is illustrated in Figure 8. It can be seen that the recombination rate is much higher at the front and back surface of the cell. However, front and back surface recombination can be reduced by adding surface passivation to the layers.

Figure 9 shows the electron and hole current densities with the variation of thickness of the device. The total output current density remained at around -18.93 mA/cm^2, which is pretty high for a p-i-n cell. This indicates that a well-designed heterojunction cell can have a higher current density and better performance.

Figure 10 illustrates the internal and external quantum efficiencies of the cell. The external quantum efficiency reached a maximum of 96.29% at wavelength (λ) of around 630 nm. The overall external quantum efficiency remained very high from 85-95 % for wavelength of 300-650 nm range. This indicates that the device will perform its best under both high and low frequency i.e. ultra-violet, near visible, and visible light wavelengths. Figure 10 shows the spectral response of the cell which also indicates the similar scenario.

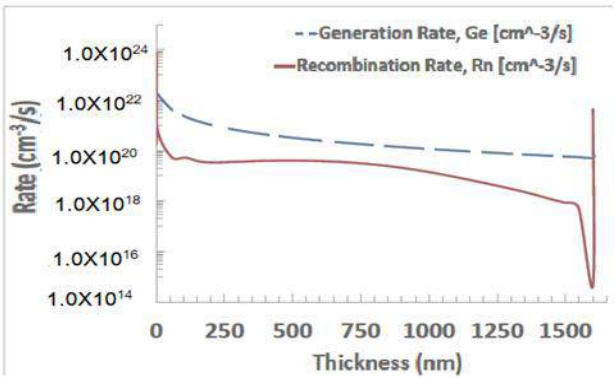

Fig. 8. Generation and recombination rate of the best performed cell

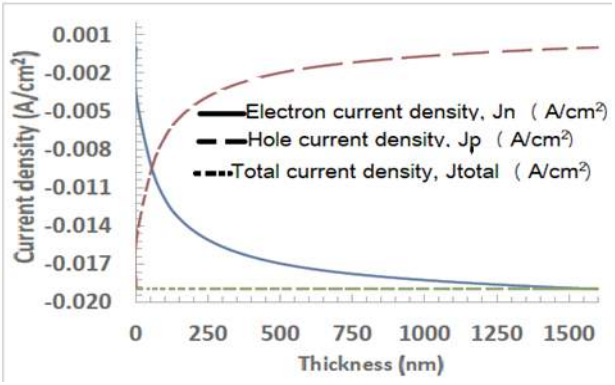

Fig. 9. Current density of the a-Si:H/μc-Si:H heterostructure p-i-n cell

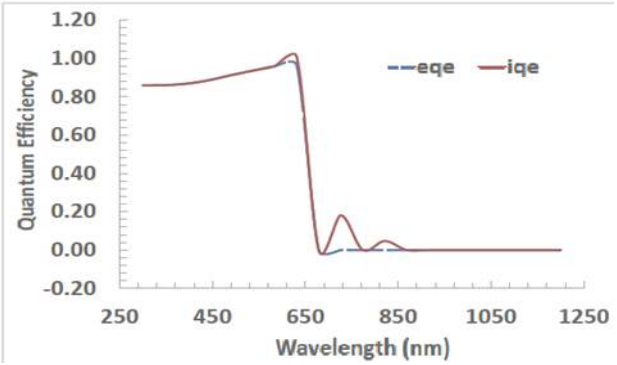

Fig. 10. Internal and external quantum efficiency of the p-i-n cell

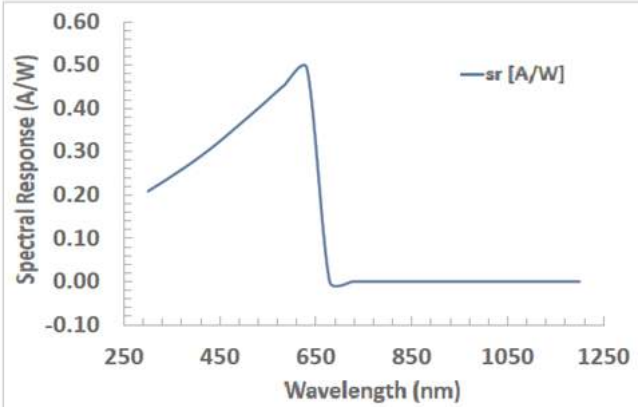

Fig. 11. Spectral response of the optimal heterojunction cell

IV. Conclusions

The parameters like bandgap, layer thickness, and doping concentrations of aSi:H/μc-Si:H heterojunction p-i-n cell are varied with AFORS-HET simulation software. It is found that layer thicknesses have significant effects on efficiency improvement. With increase in thickness of p-layer the amount of light reaching the absorber layer reduces and results in lower J_{SC} values. It also becomes difficult for the built in field to separate the electron-hole pair if the thickness of p-layer is high. Therefore, a thin a-Si:H p-layer of 1 to 5 nm would result in a better J_{SC}, and V_{OC}, and thus a higher efficiency. A thick a-Si:H absorber layer of 1400 to 1800 nm should be used to get better performance from the device. Finally, for μc-Si:H n-layer the maximum efficiency can be achieved within 1 to 10 nm range. Although J_{SC} decreases

with increase of thickness of n-layer V_{OC} remains constant throughout the variation. The doping concentrations of both a-Si:H p-, and μc-Si:H n-layers are varied and maximum efficiency of around 14.77% is achieved with acceptor concentration of 1×10^{21} cm^{-3} and donor concentration of 1×10^{20} cm^{-3}. The bandgap of p-, i-, and n-layers are also varied and optimum performance is found at higher bandgaps closer to 2.2 eV for a-Si:H p-layer, 1.85 eV for a-Si:H i-layer, and 1.2 eV for μc-Si:H n-layer.

Finally, using these values an optimum cell is numerically designed and simulated. It is found that the best-performed cell has a short circuit current density of -18.93 mA/cm^2, open circuit voltage of -1095 mV, fill factor of 0.7124, and efficiency of 14.77%. The cell has higher front and back surface recombination speeds which can be reduced by surface passivation. Besides this, the cell has maximum external quantum efficiency of 96.29% at wavelength (λ) of around 630 nm. The overall external quantum efficiency remained very high from 85-95% for wavelength of 300-650 nm range. This indicates that the device will perform its best under both high and low frequency i.e. ultra-violet, near visible, and visible light wavelengths.

References

1. Soga Tetsuo, 2006. Nanostructured Materials for Solar Energy Conversion, 1st Edition, Elsevier.
2. Gaspari Franco, Simone Quaranta, 2018. Comprehensive Energy Systems. Chapter 2: PV Materials, **2**, 117-149.
3. Hossain Mohammad Kamal, 2015. Hydrogenated Amorphous Silicon-Based Thin Film Solar Cell: Optical, Electrical and Structural Properties. Advanced Materials Research, **1116**, 59-64.
4. Kang H., 2021. Crystalline Silicon vs. Amorphous Silicon: the Significance of Structural Differences in Photovoltaic Applications. *IOP Conf. Series: Earth Environ. Sci., **726**, 012001.*
5. Bhattacharya Pallab, Roberto Fornari and Hiroshi Kamimura, 2011. Section 2: Materials, Preparation and Properties, Comprehensive Semiconductor Science and Technology. 1st Edition, Elsevier Science.
6. Bhattacharya Sayak and Sajeev John, 2019. Beyond 30% Conversion Efficiency in Silicon Solar Cells: A Numerical Demonstration. Scientific reports, Nature Research, **9**(1), 1–15.
7. Sark Wilfried van, L. Korte, and F. Roca, 2012. Physics and technology of amorphous crystalline heterostructure silicon solar cells. Engineering Materials book series, Springer.
8. Fahrner W. R., 2013. Amorphous silicon/ crystalline silicon heterojunction solar cells. Engineering Materials book series, Springer.
9. Nayfeh Munir, 2018. Fundamentals and Applications of Nano Silicon in Plasmonics and Fullerines. 1st Edition, Elsevier.
10. Pieters B. E., H. Stiebig, M. Zeman, and R. A. C. M. M. van Swaaij, 2009. Determination of the mobility gap of intrinsic μc-Si:H in p-i-n solar cells. Journal of Applied Physics, **105**, 044502.
11. Shi Donglu, Zizheng Guo and Nicholas Bedford, 2015. Nanomaterials and Devices, Micro and Nano Technologies. Nanoenergy Materials, 255-291.
12. Yunaz I. A., A. Yamada, and M. Konagai, 2007. Theoretical analysis of amorphous silicon alloy based triple junction solar cells. Japanese Journal of Applied Physics, **46**, 1152.
13. Meier J., J. Spitznagel, S. Fay et al., 2002, Enhanced light-trapping for micromorph tandem solar cells by LP-CVD ZnO. *Proceedings of the 29th IEEE Photovoltaic Specialists Conference, 1118–1121*.
14. Yamamoto K., A.Nakajima, M. Yoshimi et al., 2004. A high efficiency thin film silicon solar cell and module. Solar Energy, **77**(6), 939–949.
15. Yan B., G. Yue, L. Sivec, J. Yang, S. Guha, and C.-S. Jiang, 2011. Innovative dual function nc-SiO_x:H layer leading to a>16% efficient multi-junction thin-film silicon solar cell. Applied Physics Letters, **9**, 113512.
16. Green M. A., E. D. Dunlop, J. Hohl-Ebinger, M. Yoshita, N. Kopidakis, and X. Hao, 2021. Solar cell efficiency tables (version 57), Prog. Photovolt. Res. Appl., **29**, 3– 15.
17. Ding K., U. Aeberhard, F. Finger, and U. Rau, 2013. Optimized amorphous silicon oxide buffer layers for silicon heterojunction solar cells with microcrystalline silicon oxide contact layers. *Journal of Applied Physics, **113** (13), 134501.*
18. Ge J., Z. Ling, J. Wong, T. Mueller, and A. Aberle, 2012. Optimization of intrinsic a-Si: H passivation layers in crystalline-amorphous silicon heterojunction solar cells. *Energy Procedia, **15**, 107-117.*
19. Singh Jasprit, 2000. Semiconductor Devices: Basic Principles. John Wiley & Sons.
20. Green Martin A., 1982. Solar Cells: Operating Principles, Technology, and System Applications. Englewood Cliffs: Prentice-Hall, Inc.
21. https://www.helmholtz-berlin.de/, Accessed on 7 September 2021.
22. Matsui T., M. Kondo, K. Ogata, T. Ozawa, and M. Isomura, 2006. Influence of alloy composition on carrier transport and solar cell properties of hydrogenated microcrystalline silicon-germanium thin films. Applied Physics Letters, **89**, 142115.
23. Shah A., 2010. Thin film silicon solar cells. EPFL press, Switzerland.
24. Burdorf S., G. H. Bauer, and R. Bruggemann, 2012. Numerical simulations on the limits for the efficiency improvement of hybrid dye-microcrystalline silicon solar cells. *Solar Energy Materials and Solar Cells, **99**, 345-348.*
25. Sharma M., S. Kumar, N. Dwivedi, at el., 2013. Optimization of band gap, thickness and carrier concentrations for the development of efficient microcrystalline silicon solar cells: A theoretical approach. *Solar Energy, **97**, 176-185.*
26. Huang J., C. W. Hsu, J. Shieh, et al., 2010. Device modeling of a micromorph tandem solar cell using AMPS-1D, *35th IEEE Photovoltaic Specialists Conference, 1512-1515.*
27. Nath M., S. Chakraborty, E. Johnson, et al., 2011. Factors limiting the open-circuit voltage in microcrystalline silicon solar cells. *EPJ Photovolt, **2**, 20101, 1-12.*